

Journal of Materials Chemistry A

Accepted Manuscript



This is an *Accepted Manuscript*, which has been through the Royal Society of Chemistry peer review process and has been accepted for publication.

Accepted Manuscripts are published online shortly after acceptance, before technical editing, formatting and proof reading. Using this free service, authors can make their results available to the community, in citable form, before we publish the edited article. We will replace this *Accepted Manuscript* with the edited and formatted *Advance Article* as soon as it is available.

You can find more information about *Accepted Manuscripts* in the [Information for Authors](#).

Please note that technical editing may introduce minor changes to the text and/or graphics, which may alter content. The journal's standard [Terms & Conditions](#) and the [Ethical guidelines](#) still apply. In no event shall the Royal Society of Chemistry be held responsible for any errors or omissions in this *Accepted Manuscript* or any consequences arising from the use of any information it contains.



Journal Name

ARTICLE

Hierarchical nanosheet-based CoMoO₄-NiMoO₄ nanotubes for applications in asymmetric supercapacitor and oxygen evolution reaction†

Received 00th January 20xx,
Accepted 00th January 20xx

DOI: 10.1039/x0xx00000x

www.rsc.org/

Zhuoxun Yin,^a Yujin Chen,^{*a} Yang Zhao,^a Chunyan Li,^{*a} Chunling Zhu^{*b} and Xitian Zhang^c

Hollow structures with hierarchical architecture and multi-composition have attracted extensive interest because of their fascinating physicochemical properties as well as wide applications. Herein we report the designed synthesis of hierarchical nanosheet-based CoMoO₄-NiMoO₄ nanotubes by a hydrothermal treatment and a subsequent calcination method. The walls of hierarchical nanotubes are composed of interconnected NiMoO₄ nanosheets and CoMoO₄ nanoparticles anchored on the surface of the nanosheets. The diameter of the hollow interior, the thickness of NiMoO₄ nanosheets and the diameter of CoMoO₄ nanoparticles are around 180 nm, less than 6 nm and 3 nm, respectively, leading to the hierarchical nanotubes have a high surface area and a large pore volume. As evaluated as electrodes for pseudocapacitors, the hierarchical nanotubes with an appropriate amount of CoMoO₄ shows a high specific capacitance of 1079 F g⁻¹ at a current density of 5 A g⁻¹ and excellent stability with 98.4% capacitance retention after 1000 cycles. Furthermore, an asymmetric capacitor, consisted of active carbon and hierarchical nanosheet-based CoMoO₄-NiMoO₄ nanotubes as negative and positive electrodes respectively, delivers an energy density of 33 Wh kg⁻¹ at a power density of 375 W Kg⁻¹, and 16.3 Wh kg⁻¹ even at a high power density of 6000 W Kg⁻¹. The supercapacitive properties are much higher than those of single-phase NiMoO₄ nanotubes, most of other metal molybdates and metal oxides reported previously. Besides, the hierarchical nanotubes also exhibit much better electrocatalytic activity for oxygen evolution reaction than single-phase NiMoO₄ nanotubes, most of other metal molybdates and metal oxides. Our results demonstrate the importance of rational design of complex hollow structures with enhanced properties for a widely practical application.

1 Introduction

The limited reserves of fossil fuels and the increasing environmental pollution have stimulated intense research on energy storage and conversion from alternative energy sources.^{1,2} Systems for electrochemical energy storage and conversion include batteries, fuel cells, and electrochemical capacitors (ECs) *etc.*³ Compared with other storage devices, supercapacitors have several advantages such as a high power density, a fast charge/discharge process, a long-term stability and a low maintenance cost.⁴ According to their charge-storage mechanisms, ECs can be classified into electrical

double-layer capacitors (EDLCs) and Faradaic pseudocapacitors.⁵⁻⁷ Faradaic pseudocapacitor have much higher power density and energy density than electrical double-layer capacitor because of their fast and reversible redox reactions (several tens of nanometers from the surface). Therefore, Faradaic pseudocapacitor has attracted wide attention in recent years.⁸⁻¹³

Recent experimental result showed that metal oxides/hydroxides, conducting polymers and metal nitride could be used as pseudocapacitor electrode materials.¹⁴⁻¹⁷ Among them, metal molybdates are very promising electrode materials for high-performance ECs because of their feasible oxidation states.¹⁸⁻²¹ For example, Wan *et al* synthesized NiMoO₄·H₂O nanoclusters, which exhibited a capacitance of 680 F g⁻¹ at a current density of 1 A g⁻¹ and less than 60 % of the initial capacitance could be retained after 1000 cycles.¹⁹ Liu *et al* demonstrated that CoMoO₄ nanorods had a high capacitance of 286 F g⁻¹ at a current density of 5 mA cm⁻².²⁰ However, the rate capability and long-term stability of some single-phase metal molybdates are unsatisfactory.^{18,19,21} Recently, mixed metal molybdates exhibited enhanced rate capability compared to single-phase metal molybdates due to the synergistic effect.²²⁻²⁴ For instance, hierarchical MnMoO₄-CoMoO₄ nanowires had a capacitance of 187.1 F g⁻¹ at a current density of 1 A g⁻¹, great higher than both single-phase

^aKey Laboratory of In-Fiber Integrated Optics, Ministry of Education and College of Science, Harbin Engineering University, Harbin 150001, China. E-mail: chen yujin@hrbeu.edu.cn and chunyanli@hrbeu.edu.cn; Fax: +86-451-82519754; Tel: +86-451-82519754.

^bCollege of Materials Science and Chemical Engineering, Harbin Engineering University, Harbin 150001, China. E-mail: zhuchunling@hrbeu.edu.cn

^cKey Laboratory for Photonic and Electronic Bandgap Materials, Ministry of Education, and School of Physics and Electronic Engineering, Harbin Normal University, Harbin 150025, China.

†Electronic Supplementary Information (ESI) available: [Structural characterizations, nitrogen adsorption and desorption isotherms and the corresponding pore-size distributions of NCMNTs and NMNT. SEM images of samples with excessive cobalt chloride, cobalt acetate, and without nickel acetate. Tafel plots of NCMNT-3 and NMNT. Comparisons of the electrochemical properties of NCMNTs with other active materials]. See DOI: 10.1039/x0xx00000x

MnMoO₄ and CoMoO₄ nanowires. Moreover, the MnMoO₄-CoMoO₄ nanowires exhibited a very good long-term stability.²² Liu *et al* synthesized CoMoO₄-NiMoO₄·xH₂O bundles by a chemical co-precipitation method. The mixed bundles showed a capacitance of 1039 Fg⁻¹ at a current density of 1 A g⁻¹ and excellent rate capability, superior to single-phase NiMoO₄·xH₂O.²³ Besides, it is also necessary for high-performance pseudocapacitor electrode materials to have a high surface area since pseudocapacitive behavior occurs (charges stored in electrode materials) only within few nanometres from the surface of the electrode materials. Therefore, the nanostructures with an ultrathin thickness or a high surface area for next generation high performance supercapacitors are highly desired. However, the surface areas of most of mixed metal molybdates reported previously are relatively low, limiting their supercapacitive properties.

On the other hand, the energy density (*E*) of the pseudocapacitors as the next-generation energy storage devices is still unsatisfactory. The energy density can be efficiently enhanced by constructing asymmetric supercapacitor according to the following equation,

$$E = 1/2CV^2 \quad (1)$$

where *C* is the specific capacitance, and *V* is the cell voltage.¹⁰ Therefore, it is necessary to investigate the electrochemical capacitive performance of asymmetric supercapacitors based on the designed active material.

Electrolytic water splitting holds the promise for global scale storage and conversion of renewable energy.^{25,26} However, electrocatalysts are usually required because of the sluggish kinetics of OER caused by the involved multi proton-couple electron transfer steps. Oxides of iridium and ruthenium showed high catalytic activity toward OER, but their high cost and scarcity restricted their application on the scale.²⁷⁻²⁹ Therefore, it is highly desirable and imperative to exploit new OER catalysts with high catalytic activity and low cost.³⁰⁻³⁴ Recently, metal molybdate nanostructures as electrocatalysts for OER have been reported in an alkaline solution; however, the OER performance of single-phase metal molybdate nanostructures is unsatisfactory due to similar reasons to those as they are used as electrodes of ECs.^{35,36}

Herein, we develop a facile strategy to fabricate hierarchical NiMoO₄-CoMoO₄ nanotubes (NCMNTs) consisted of ultrathin and mesoporous NiMoO₄ nanosheets and CoMoO₄ nanoparticles on the surface of the NiMoO₄ nanosheets. The hierarchical nanotubes as pseudocapacitor electrode materials have the following advantages. (i) The surface area of the hierarchical nanotubes is greatly larger than those of mixed metal molybdates reported previously. Moreover, the thickness of the ultrathin nanosheets is less than 6 nm, which makes active sites on the surface of the nanosheets expose to electrolyte fully. (ii) Interconnected network is formed among the nanosheets, which can enhance the stability of structure during the charging and discharging processes. (iii) The introduction of CoMoO₄ decreases the charge transfer resistance of the hierarchical nanotubes, which facilitates the enhancement of the rate capability. (iv) The special structural features of the hierarchical nanotubes including a tube-like

morphology and mesopores in the nanosheets can offer more ion pathways, and thereby improve the ion transport kinetics of electrode materials. As a result, the NCMNTs as supercapacitor electrode materials exhibit excellent electrochemical properties including high special capacitance and good rate capability. In order to improve the energy density of the hierarchical nanotubes, we also fabricate asymmetric supercapacitor (active carbon (AC) // NCMNT), exhibiting enhanced energy density compared to those of asymmetric supercapacitors based on single counterparts and other metal oxides as positive electrodes.^{10,17,18,23,24} In addition, the NCMNTs can be used as electrocatalysts for oxygen evolution reaction (OER), also exhibiting superior catalytic activity to other metal (Fe, Co, Ni) molybdates and metal oxides reported previously.³²⁻⁴⁸

2 Experimental section

2.1 Synthesis of hierarchical NCMNTs

The hierarchical NCMNTs were synthesized through the following two steps. 75 mg of MoO₃ nanorods, 620 mg of nickel acetate, and cobalt chloride with a different weight were dispersed in 35 mL water-ethanol (volume ratio = 1: 1) solvent under sonication for 20 min. The mixture was pour into a 40 ml Teflon-lined stainless steel autoclave for thermal treatment at 90°C for 5 h. As the autoclave cooled to room temperature, the precipitates were washed with distilled water and absolute ethanol seven times, and dried in air at 60°C. The precursors were annealed in an air atmosphere at 500°C for 2 h, and then the hierarchical NCMNTs were synthesized successfully. The samples obtained with added weights of cobalt chloride of 85 mg, 75 mg and 65 mg were named as NCMNT-1, NCMNT-2 and NCMNT-3, respectively. For comparison, the pure hierarchical NiMoO₄ nanosheet-based nanotubes (NMNT) were also prepared through our previous method with simple modification.²¹

2.2 Structure characterization

The samples were characterized by a scanning electron microscope (SEM; HITACHI SU8000) and transmission electron microscopy (TEM; FEI Tecnai-F20) equipped with a Gatan Imaging Filter (GIF). The crystal structure of the sample was determined by X-ray diffraction (XRD) [D/max 2550 V, Cu K α radiation]. The pore diameter distribution and surface area were tested by nitrogen adsorption/desorption analysis (TRISTAR II3020). ICP mass spectrometry was measured by Thermo iCAP 6000 ICP-MS.

2.3 Electrochemical measurements

Electrochemical supercapacitor measurements were performed in a three-electrode electrochemical cell containing 2 M KOH aqueous solution as the electrolyte. Cyclic voltammetry and galvanostatic charge-discharge curves were carried out using a CHI660D electrochemical workstation. A platinum foil and saturated calomel electrode (SCE) were used as counter and reference electrodes, respectively. The working electrode was prepared as follows: 75 wt% of the active

material, 15 wt% of acetylene black, and 10 wt% of polytetrafluoroethylene were mixed under sonication until a homogeneous black slurry was obtained. The slurry was pressed into a nickel foam, and then dried at 60°C for 12 h. The working electrode with a geometric surface area of 1 cm² contained 2.6 mg of NCMNTs.

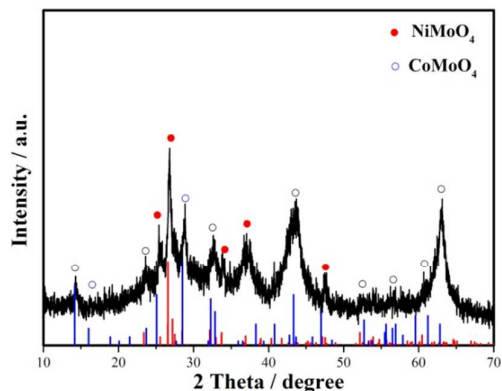


Fig. 1 XRD pattern of the hierarchical nanosheet-based NCMNT-3 nanotubes

The asymmetric supercapacitor with NCMNTs-3 as a positive electrode and AC as a negative electrode was assembled with a porous polymer membrane separator. The negative electrode was prepared as follows: AC (80 wt%), MWNT (10 wt%) and polyvinylidene fluoride (PVDF) (10 wt%) were mixed under sonication until a homogeneous black slurry was obtained. The slurry was pressed into nickel foam, and then dried at 90°C for 12 h. The negative electrode with a geometric surface area of 1 cm² contained 8.7 mg of AC. A 2 M KOH solution was employed as electrolyte for the two-electrode measurements.

The specific capacitance values of the electrode were calculated from galvanostatic charge–discharge curves according to Equation 2,

$$C_s = i\Delta t / m\Delta V \quad (2)$$

where C_s (F g⁻¹) is the specific capacitance, i (A) is the discharge current, Δt (s) is the discharge time, m (g) is the weight of the active materials, and ΔV is the voltage interval of the discharge. The power density of the asymmetric supercapacitor was calculated by Equation 3,

$$P = E / \Delta t \quad (3)$$

The OER activities of NMNT and NCMNTs were carried out using a CHI660D electrochemical workstation with a standard three-electrode cell in 1 M KOH aqueous solution. The working electrode is prepared through the same method for the preparation of the supercapacitor electrode, but the loading weight is around 7 mg. A platinum foil and a Ag/AgCl electrode were used as counter and reference electrodes, respectively. The polarization curves were recorded by linear sweep of potential a scan rate of 1 mV s⁻¹. All data have been corrected with iR compensation based on impedance spectroscopy. The measured potentials were also referred to reversible hydrogen electrode (RHE) with the following equation: $E_{\text{RHE}} = E_{\text{Ag/AgCl}} + 0.059 \times \text{pH} + 0.21$.

3 Results and discussion

3.1 Structural characterization

The MoO₃ nanorods used in this work have a diameter and a length of around 170 nm and several micrometers, respectively.^{49–51} The information about the crystal phase and structure of the NCMNTs was obtained by XRD measurements. Fig. 1 shows a typical XRD pattern of NCMNT-3. By comparison of the measured result with the data from the Joint committee on powder diffraction standards (JCPDS), we find that the diffraction peaks come from monoclinic NiMoO₄ (JCPDS, card no. 45-0142, cell parameters: $a = 1.0184$ nm, $b = 0.8734$ nm, $c = 0.7649$ nm, $\beta = 107.095^\circ$) and monoclinic CoMoO₄ (JCPDS, card no. 25-1434, cell parameters: $a = 0.967$ nm, $b = 0.885$ nm, $c = 0.776$ nm, $\beta = 113.082^\circ$), respectively. The weak intensities of the diffraction peaks indicate poor crystallizations of both NiMoO₄ and CoMoO₄ in NCMNT-3. The poor crystallizations of the NCMNTs may be favorable for the increments in their electrochemical performance because of more defects presented in the active materials with a weak crystallinity.¹⁷

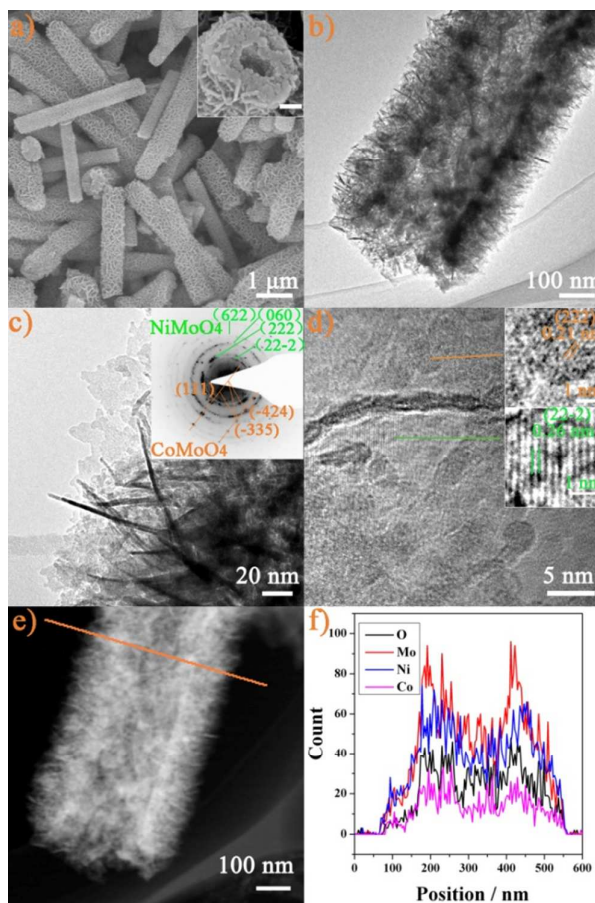


Fig. 2 Structural characterization of the hierarchical NCMNT-3. (a) SEM image, the inset showing the tubular characteristic of the products, and the scale bar: 100 nm, (b) and (c) TEM images, and the inset showing the SAED pattern, (d) HRTEM image, and the scale bar in the inset: 1 nm, (e) ADF-STEM image and (f) linear EDX spectrum.

The morphology and the microstructure of NCMNT-3 were characterized by SEM and TEM measurements. Fig. 2(a) shows SEM image of NCMNT-3. It can be found that many nanosheets branch out from the surface of NCMNT-3, forming an interesting three-dimensional (3D) hierarchical architecture. The nanosheets connect to each other and form a network-like structure, leading to the formation of void space among the nanosheets. On one hand, the network-like structure is favorable for the structural stability of NCMNTs during long-term electrochemical measurements. On the other hand, abundant void space among the interconnected nanosheets can make NCMNT-3 fully accessible to electrolyte. Compared to the initial MoO_3 nanorods, the diameter of the 3D hierarchical architecture is increased to 400–600 nm, but its length is decreased to around 3.5 μm , as shown in Fig. 2(a). The increased diameter is due to foreign materials grown along the radial direction, and the shorten length is due to the alkali etching effect.²¹ The inset in Fig. 2(a) displays that the central parts of NCMNT-3 exhibits a hollow character, suggesting NCMNT-3 has a tube-like morphology. This can be further confirmed by TEM observation, as shown in Fig. 2(b). From the TEM image, the diameter of the hollow interior of NCMNT-3 is around 180 nm, and the height of the interconnected nanosheets is about 120 nm. High-magnification TEM image (Fig. 2(c)) shows the average thickness of the nanosheets is less than 6 nm. Interestingly, not only diffraction rings but also diffraction dots can be observed clearly in the selected area electron diffraction (SAED) pattern, as shown in the inset of Fig. 2(c) and Fig. S1.† By careful measurements, the labeled diffraction rings can be indexed to the (22-2), (222), (060), and (622) planes of monoclinic NiMoO_4 phase, whereas the labeled diffraction dots are indexed to the (111), (-335) and (-424) planes of monoclinic CoMoO_4 phase, which is consistent with the XRD analysis. The atomic ratio of Ni to Co was determined by ICP-MS measurements to be about 9.5:1. The total molar quantities of Ni and Co are larger than that of Mo, indicating that residue MoO_3 is not left in NCMNT-3. Fig. 2(d) displays a high-magnification TEM image taken from a basal plane of the nanosheets. It can be found that there are small particles with a size of around 5 nm anchored on the surface of the basal plane. The upper inset of Fig. 2(d) shows a high-resolution TEM (HRTEM) taken from small particles. The labeled lattice distance is 0.21 nm, corresponding to (222) plane of monoclinic CoMoO_4 phase. The marked lattice distance of the smooth surface of the nanosheets without small particles is 0.26 nm, corresponding to (22-2) plane of monoclinic NiMoO_4 phase. Thus, the hierarchical NCMNTs are composed of ultrathin NiMoO_4 nanosheets and CoMoO_4 nanoparticles anchored on the surface of the nanosheets. Besides CoMoO_4 nanoparticles, there are small pores in the surface of NiMoO_4 nanosheets, as shown in Fig. S2.† In order to further determine the elemental distribution in NCMNTs, annular dark-field (ADF) scanning transmission electron microscopy (STEM, Fig. 2(e)) and the corresponding linear scanning energy dispersive X-ray spectrometry (EDX) (Fig. 2(f)) were carried out. As shown in Fig. 2(f), Mo, Ni, Co and O elements distribute

at the whole region of the NCMNTs, however, their quantities are much higher in the external region than in the inner one. This not only further confirms the elemental composition, but also the tubular character of NCMNTs. STEM image and the corresponding EDX elemental mappings show that NiMoO_4 and CoMoO_4 mainly distributes in the nanosheets (Fig. S3), but the amount of CoMoO_4 is less than that of NiMoO_4 . †

The SEM and TEM observations show that NCMNT-3 with a tubular character consists of the interconnected NiMoO_4 nanosheets with small CoMoO_4 nanoparticles anchored on the nanosheets, suggesting it has a large surface area. In terms of its nitrogen adsorption–desorption isotherms, Brunauer–Emmett–Teller (BET) surface area of NCMNT-3 was calculated to be 186.7 $\text{m}^2 \text{g}^{-1}$ (Fig. S4(a)), which is much higher than those of CoMoO_4 – NiMoO_4 composites reported previously.^{23,24} In addition, the hierarchical nanotubes exhibited a type IV hysteresis, indicating the presence of mesoporous structure. The average pore diameter and cumulative volume of pores calculated from the adsorption branch of the nitrogen isotherm using the Barrett–Joyner–Halenda (BJH) method are about 17.4 nm and is 0.97 $\text{cm}^3 \text{g}^{-1}$, respectively, as shown in Fig. S4(b).† Moreover, the pore size distribution of NCMNT-3 exhibits a bimodal distribution with a narrow distribution centered at 10 nm and a broaden distribution centred at 120 nm. The small pore may be associated to pores in NiMoO_4 nanosheets and the larger pore is originated from hollow interior of NCMNT-3. The porous and hollow character of NCMNTs with a large surface area and large pore volume is favoured in supercapacitor applications since it provides not only larger contact area between electrode and electrolyte for shortening the charge diffusion pathway, but also more active sites for taking part in redox reactions.

In order to investigate the effect of the added weight of cobalt chloride on the structure and morphology of the products, a series of compared experiments were carried out. We noted that NCMNTs could successfully be fabricated as the added weight of cobalt chloride is ranging from 65 to 85 mg. As mentioned above, the obtained samples, as the added weights of cobalt chloride changed to 85 and 75 mg, are named as NCMNT-1 and NCMNT-2, respectively. XRD (Fig. S5) and SEM (Fig. S6) analyses show that they have similar phase compositions and morphologies to NCMNT-3.† ICP-MS measurements display that the atomic ratio of Ni and Co for NCMNT-1 was about 7.5:1 and about 8.4:1 for NCMNT-2. The nitrogen adsorption–desorption isotherms (Fig. S7 and Fig. S8) shows that the BET surface areas of NCMNT-1 and NCMNT-2 are 112.7 and 131.1 $\text{m}^2 \text{g}^{-1}$, respectively.† The average pore diameter and cumulative volume of pores are about 15.5 nm and 0.43 $\text{cm}^3 \text{g}^{-1}$ for NCMNT-1, and about 17.3 nm and 0.68 $\text{cm}^3 \text{g}^{-1}$ for NCMNT-2, respectively. However, the added weight of cobalt chloride exceeded to 95 mg, two kinds of precipitates with different colors would be formed in the precursors. SEM image (Fig. S9(a)) displays that besides the hierarchical nanotubes, 2D nanosheets are also formed in the precursors.† Moreover, the amount of 2D nanosheets was increased with the further increase of the weight of cobalt chloride (i.e. 590 mg), as shown in Fig. S9(b).† This suggests that uniform

NCMNTs could not be formed if the added weight of cobalt chloride exceeded to 95 mg. On the other hand, any materials could not be grown on the surface of MoO_3 nanorods without nickel acetate in the reaction system, as shown in Fig. S10.† As discussed in our previous report,²¹ it is associated with the formation mechanism of the hierarchical nanosheets-based nanotubes. Such hierarchical nanotubes were only produced in a weak alkaline solution. However, the water-ethanol solvent only containing cobalt chloride cannot provide a weak alkaline condition. Thus under the condition, the hierarchical nanotubes could not be obtained. If cobalt chloride was replaced with cobalt acetate, the hierarchical CoMoO_4 - NiMoO_4 nanotubes would be obtained, as shown in Fig. S11a and 11b).† However, the length of the nanotubes decreased significantly due to the enhanced alkalinity of the solution (Fig. S11b).† In addition, we tried to synthesize the hierarchical CoMoO_4 nanotubes using MoO_3 nanorods and cobalt acetate as precursors in the water-ethanol (volume ratio = 1: 1) system, however, the experimental results showed that the hierarchical CoMoO_4 nanotubes could not be fabricated successfully, as shown in Fig.S12.†

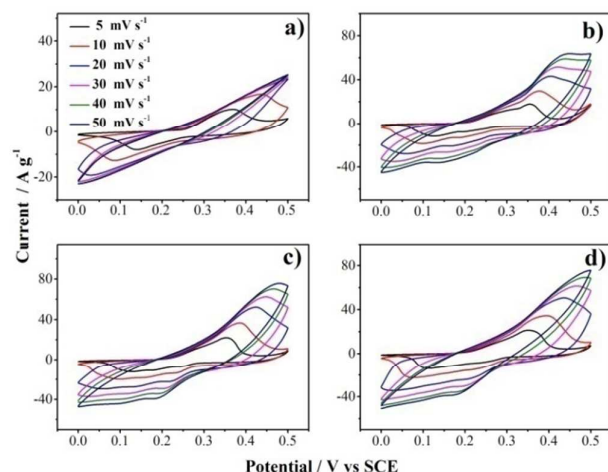


Fig. 3 The CV curves of different samples. (a) NMNT, (b) NCMNT-1, (c) NCMNT-2 and (d) NCMNT-3

3.2 Electrochemical supercapacitive performance

The electrochemical performance of the hierarchical NCMNTs as supercapacitor electrodes was evaluated using a three-electrode configuration in 2 M KOH solution as the electrolyte. Fig. 3 shows the cyclic voltammetry (CV) curves of the NMNT and NCMNTs at various scan rates in the potential range of 0–0.5 V vs SCE. Significant redox peaks can be observed in each curve, suggesting that the measured capacitances of all the hierarchical nanotubes are mainly based on the pseudocapacitive mechanism. The intensities of the redox current peaks increase with an increase of the scan rate, suggesting a surface-controlled electrochemical process, i.e., the kinetics of the interface Faradic redox reactions. With increasing scan rate, the oxidation peak shifts towards a more positive potential and the reduction peak shifts towards a more negative potential. This is attributed to an increase of

the internal diffusion resistance within the active material with an increase in scan rate.^{15,16} Even at a high scan rate (50 mV s^{-1}), the redox peaks are still evident, suggesting that the NCMNTs as the cathodes for ECs are stable and have good rate capability.

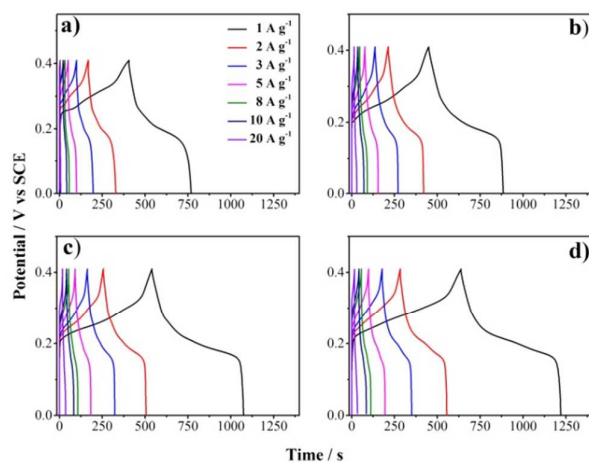


Fig. 4 The galvanostatic charge-discharge curves of different samples. (a) NMNT, (b) NCMNT-1, (c) NCMNT-2 and (d) NCMNT-3.

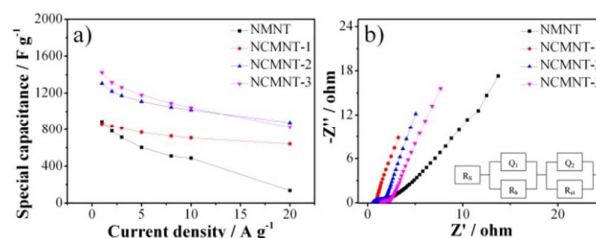


Fig. 5 (a) The specific capacitances of NMNT and NCMNTs at various current density and (b) the Nyquist plots of NMNT and NCMNTs and the inset showing corresponding model.

Fig. 4 shows the galvanostatic charge-discharge curves of the NMNT and NCMNTs at various current densities at room temperature. The specific capacitances were calculated from the discharge curves according to Equation (2), and the calculated values are shown in Fig. 5(a) and Table S1. As shown in Fig. 5 and Table S1, NCMNT-2 and NCMNT-3 show comparable electrochemical supercapacitive performance, and their specific capacitances are 1307 and 1424 F g^{-1} at 1 A g^{-1} , respectively, greatly larger than that of NMNT (887 F g^{-1}). Although the capacitance of NCMNT-1 (865 F g^{-1}) at 1 A g^{-1} is slightly smaller than that of NMNT, all of the NCMNTs exhibit better rate capabilities than NMNT. When the current density increased from 1 to 20 A g^{-1} , nearly 58.1, 67.2 and 74.2% of the initial capacitance value of NCMNT-3, NCMNT-2 and NCMNT-1 still remained; however, only 14.6% of the initial capacitance value of NMNT retained. Thus, it can be concluded that CoMoO_4 with appropriate amount in NCMNTs not only can improve the capacitance value, but also significantly enhance the rate capability of NCMNTs. Furthermore, with an increase of the amount of CoMoO_4 , the capacitance of NCMNTs decreased, but the rate capability improved, which is consistent with the previous results reported by Liu *et al.*²³ Thus, NCMNT-3 show superior electrochemical properties,

including higher specific capacitance and better rate capability, to NMNT. Importantly, compared to other metal molybdates and metal oxides, NCMNT-3 also exhibited excellent electrochemical performance, as shown in Table S1.¹⁵⁻²⁴ The enhanced supercapacitive performance of NCMNTs is due to the following points. (i) It is attributed to the synergistic effect between NiMoO₄ and CoMoO₄ active materials since both NiMoO₄ and CoMoO₄ contributes to the total capacitances.^{23,24} (ii) The surface areas of NCMNTs are larger than those of NMNT, other metal molybdates and metal oxides,^{17,21-24} allowing NCMNTs to provide more active sites for the redox reactions. (iii) The introduction of CoMoO₄ in the NCMNTs can increase the conductivity of cathodes, which favors in the enhancement of the rate capability. This is evidenced by the electrochemical impedance spectroscopy (EIS). Fig. 5(b) shows the Nyquist plots of NCMNTs and NMNT. Each plot shows a semicircle in a high-frequency region and a straight line in the low-frequency region, suggesting that light electrochemical polarization and good capacitive properties. As fitted from the experimental data by a model (the inset in Fig. 5(b)), the charge-transfer resistances can be obtained. The fitted results show that NCMNT-3 electrode has smaller charge-transfer resistance (1.035 Ω) than those of NMNT (1.544 Ω), NCMNT-1 (1.299 Ω) and NCMNT-2 (1.14 Ω) electrodes. In addition, NCMNTs have more vertical straight lines than that of NMNT, indicating that NCMNTs have lower diffusive resistances to the electrolyte and faster ion transport speeds than those of NMNT.

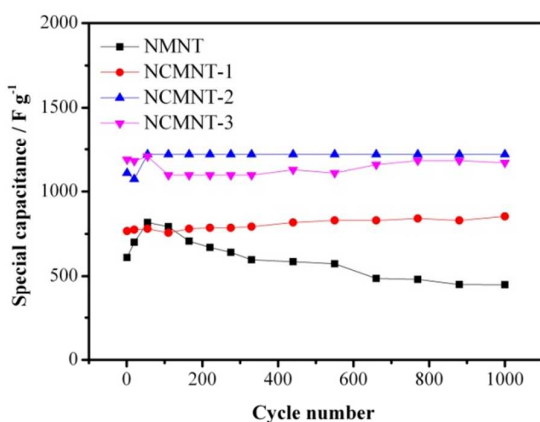


Fig. 6 The cycling stability of NMNT and NCMNTs at a current density of 5 A g⁻¹.

The cycling stabilities of NCMNTs and NMNT were evaluated using a long-term galvanostatic charge–discharge process (Fig. 6). The capacitances of NCMNTs and NMNT increased at the first cycle to the 55th cycle, which may be associated to the activation of the active materials. After around 1000 cycles the capacitances of NCMNTs stabilized, and capacitance retentions of 111%, 109% and 98.4% were achieved for NCMNT-1, NCMNT-2 and NCMNT-3 at a current density of 5 A g⁻¹; however, capacitance retention of NMNT (the initial capacitance of 603 F g⁻¹) is only 74.6%. This implies NCMNTs exhibit better electrochemical stability than NMNT.

Due to better overall electrochemical supercapacitive performance of NCMNT-3, we used it as positive electrode to assemble an asymmetric supercapacitor (ASC) with AC as the negative electrodes. Fig. 7(a) shows CV curves of AC and

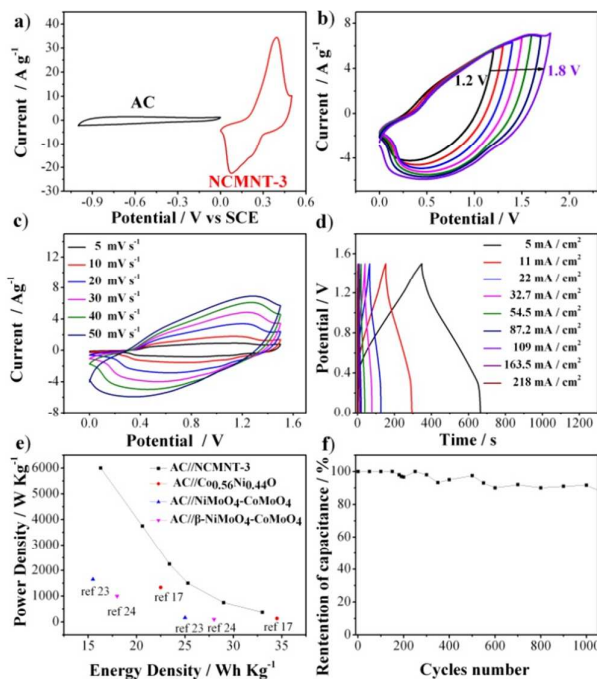


Fig. 7 (a) CV curves of AC and NCMNT-3 measured in a three-electrode device in 2M KOH aqueous solution at a scan rate of 10 mVs⁻¹, (b) CV curves of as-fabricated ASC at different operation voltages and at a scan rate of 50 mV s⁻¹, (c) CV curves of the as-assembled ASC at different scan rates, (d) Galvanostatic charge/discharge curves of the ASC device, (e) Ragone plot of the ASC device and (f) cycling performance of the ASC device at 50 mA cm⁻².

NCMNT-3 at a scan rate of 10 mVs⁻¹, which indicate that the stable voltage for AC is between -1.0 and 0 V with a EDLC behavior, and between 0 and 0.5 V for the NCMNT-3 with a pseudocapacitive behavior. Therefore, the operating cell voltage can be greatly enhanced when they are assembled into ASC. A series of CV curves with different voltage windows at a scan rate of 50 mVs⁻¹ were measured to estimate the operating potential of ASC cell. As shown in Fig. 7(b), the potential window for ASC may be extended to 1.8 V. However, the galvanostatic charge–discharge curves at 5 mA under a potential exceeding 1.6 V in 2 M KOH solution demonstrate distinct asymmetry between charge and discharge curves (Fig. S13). Thus, we determine the potential window for ASC to be 1.5 V. Fig. 7(c) shows the CV curves of ASC at different scan rates under a potential of 1.5 V. It can be found that both pseudocapacitive and EDLC types of capacitance contribute to the total capacitance of the ASC cell. The current density increased with the scan rates, and the oxidation peak shifted to a more positive potential, similar to the phenomena observed in the three-electrode configuration. Even at a high scan rate of 50 mV s⁻¹, the redox peaks are still evident, suggesting good rate capability of the assembled ASC cell. In order to further understand the rate capability, galvanostatic charge–discharge curves at different current densities under

1.5 V in 2 M KOH solution were also carried out (Fig. 7(d)). The special capacitance calculated based on the total mass of the electrodes can reach 105 F g^{-1} at a current density of 5 mA cm^{-2} (0.5 A g^{-1}), and it still retains 52 F g^{-1} at a high current of 87 mA cm^{-2} (8 A g^{-1}), further confirming good rate capability of the ASC cell. The energy density and power density of the full cell, calculated according to Equations (1) and (3) respectively, are plotted in a Ragone plot in Fig. 7(e). The asymmetric capacitor delivers an energy density of 33 Wh kg^{-1} at a power density of 375 W Kg^{-1} , and 16.3 Wh kg^{-1} even at a high power density of 6000 W Kg^{-1} . These values are much higher than most of the reported ASC cells based on other metal molybdates and metal oxides, summarized in Table S2.^{10,17,18,22-24} Furthermore, the ASC cell exhibited good long-term cycling performance, as shown in Fig. 7(f). After 1000 cycles, the capacitance retention is up to 91.8% of the initial value. The results above demonstrate that our hybrid supercapacitor is very promising for practical application as a high power energy device.

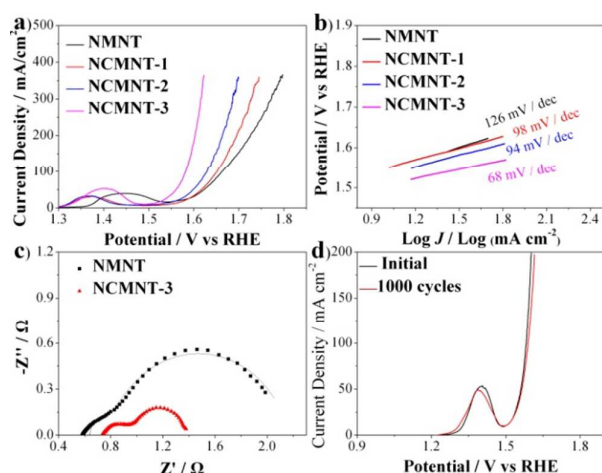


Fig. 8 (a) Polarization curves of NMNT and NCMNTs, (b) Tafel slopes of NMNT and NCMNTs, (c) the Nyquist plots of NMNT and NCMNT-3 at 1.596 V vs RHE and (d) polarization curves of NCMNT-3 before and after 1000 CV.

3.3 Electrocatalytic OER performance

NCMNTs with a high surface area and a large pore volume may exhibit good OER performance because OER generally occurs through a surface-controlled electrochemical process, similar the pseudocapacitive mechanism. Fig. 8(a) shows the polarization curves of NMNT and NCMNTs at a slow scan rate of 1 mV s^{-1} . The potential required to achieve a current density of 10 mA cm^{-2} corresponds to 10% efficient solar water-splitting devices, and thus it is a critical factor of merit for OER catalysts. It can be found that NCMNT-3 with a higher surface area exhibits a small potential of 1.530 V, greatly lower than NCMNT-1 (1.570 V), NCMNT-2 (1.557 V) and NMNT (1.589 V). Notably, NCMNT-3 shows the smallest potential value required to achieve a current density of 10 mA cm^{-2} compared to other electrocatalysts based on other metal molybdate and metal oxide nanostructures reported previously (Table S3).^{32,33,37-48} After the potentials the current densities increased sharply with the increase of the potentials, indicating good OER

catalytic activities of our catalysts. For example, to deliver a current density of 100 and 300 mA cm^{-2} NCMNT-3 requires potential of 1.585 and 1.617 V, respectively. The OER catalytic activities of NCMNT-3 outperform many other reported metal molybdate and metal oxide nanostructures. (Table S3).^{35,41,45,48} The both high current and low potential indicate that NCMNT-3 can be used as high-performance OER catalyst.

Tafel plots are applied to evaluate the efficiency of the catalytic reaction obtained from the polarization curves by the Tafel equation $\eta = b \log(j/j_0)$, where η is the overpotential, b is the Tafel slope, j is the current density, and j_0 is the exchange current density. As shown in Fig. 8(b) the NCMNT-3 exhibits a Tafel slope of 68 mV dec^{-1} , much smaller than those of NCMNT-1 (98 mV dec^{-1}), NCMNT-2 (94 mV dec^{-1}) and NMNT (126 mV dec^{-1}). This suggests a fast OER kinetics of NCMNT-3, evidenced by bubbles were clearly observed on the anode surface after the potential of 1.490 V.

To further prove OER efficiency for NMNT and NCMNT-3, EIS was conducted to study the electrode kinetics under OER condition. The Nyquist plots (Fig. 8(c)) show that the charge-transfer resistance of NCMNT-3 (0.44Ω) is smaller than that of NMNT (1.38Ω). Besides, the catalytic activity, stability is another crucial factor for OER application. The stabilities of NCMNT-3 were assessed by repeated potential cycling for 1000 cycles, as shown in Fig. 8(d). Only a slight decay of the activity (<9%) was observed referred to the polarization curves after the long-term test, implying a good stability of NCMNT-3 toward OER.

4 Conclusions

In summary, a novel strategy, involving a hydrothermal treatment and a subsequent calcination method, has been developed to synthesize hierarchical nanosheet-based $\text{CoMoO}_4\text{-NiMoO}_4$ nanotubes with high surface area. When used as the electrodes for pseudocapacitors and electrocatalysts for OER, the hierarchical nanotubes with an appropriate amount of CoMoO_4 exhibit much better electrochemical properties than single-phase NiMoO_4 nanotubes, most of other metal molybdates and metal oxides reported previously. Thus, rational design of hollow structures with hierarchical architecture and multi-composition can enhance their physicochemical properties and extend their practical application fields efficiently.

Acknowledgements

We thank the National Natural Science Foundation of China (Grant nos. 51272050 and 51572051), and also the 111 project (B13015) of the Ministry of Education of China to the Harbin Engineering University.

Notes and references

- 1 A. S. Arico, P. Bruce, B. Scrosati, J. M. Tarascon and W. V. Schalkwijk, *Nat. Mater.*, 2005, 4, 366.
- 2 Y. Huang, J. Liang and Y. Chen, *Small*, 2012, 8, 1805.

- 3 X. Zhao, B. M. Sanchez and P. J. Dobson, P. S. Grant, *Nanoscale*, 2011, 3, 839.
- 4 Y. Wang, Z. Hong, M. Wei, Y. Xia, *Adv. Funct. Mater.*, 2012, 22, 5185.
- 5 S. Chen, W. Xing, J. Duan, X. Hu and S. Z. Qian, *J. Mater. Chem. A*, 2013, 1, 2941.
- 6 G. Wang, L. Zhang and J. Zhang, *Chem. Soc. Rev.*, 2012, 41, 797.
- 7 W. Chen, C. Xia and H. N. Alshareef, *ACS Nano*, 2014, 8, 9531.
- 8 D. Choi, G. E. Blomgren and P.N. Kumta, *Adv. Mater.*, 2006, 18, 1178.
- 9 G. A. Snook, P. Kao and A. S. Best, *J. Power Sources*, 2011, 196, 1.
- 10 J. T. Zhang, J. W. Jiang, H. L. Li and X. S. Zhao, *Energy Environ. Sci.*, 2011, 4, 4009.
- 11 H. Jiang, T. Zhao, C. Z. Li and J. Ma, *J. Mater. Chem.*, 2011, 21, 3818.
- 12 J. Y. Ji, L. L. Zhang, H. X. Ji, Y. Li, X. Zhao, X. Bai, X. B. Fan, F. B. Zhang and R. S. Ruoff, *ACS Nano*, 2013, 7, 6237.
- 13 U. M. Patil, K. V. Gurav, V. J. Fulari, C. D. Lokhande and O. S. Joo, *J Power Sources*, 2009, 188, 338.
- 14 W. T. Deng, X. B. Ji, Q. Y. Chen and C. E. Banks, *RSC Adv.*, 2011, 1, 1171.
- 15 G. H. Yu, L. B. Hu, M. Vosgueritchian, H. L. Wang, X. Xie, J. R. McDonough, X. Cui, Y. Cui and Z. N. Bao, *Nano Lett.*, 2011, 11, 2905.
- 16 M. J. Zhi, A. Manivannan, F. K. Meng and N. Q. Wu, *J. Power Sources*, 2012, 208, 345.
- 17 J. W. Lang, L. B. Kong, M. Liu, Y. C. Luo and L. Kang, *J. Electrochem. Soc.*, 2010, 157, 1341.
- 18 M. C. Liu, L. Kang, L. B. Kong, C. Lu, X. J. Ma, X. M. Li and Y. C. Luo, *RSC Adv.*, 2013, 3, 6472.
- 19 H. Z. Wan, J. J. Jiang, X. Ji, L. Miao, L. Zhang, K. Xu, H. C. Chen and Y. j. Ruan, *Mater. Lett.*, 2013, 108, 164.
- 20 M. C. Liu, L. B. Kong, C. Lu, X. M. Li, Y. C. Luo and L. Kang, *Mater. Lett.*, 2013, 94, 197.
- 21 Z. X. Yin, S. Zhang, Y. J. Chen, P. Gao, C. L. Zhu, P. P. Yang and L. H. Qi, *J. Mater. Chem. A*, 2015, 3, 739.
- 22 L. Q. Mai, F. Yang, Y. L. Zhao, X. Xu, L. Xu and Y. Z. Luo, *Nat. Commun.*, 2011, 2, 381.
- 23 M. C. Liu, L. B. Kong, C. Lu, X. J. Ma, X. M. Li, Y. C. Luo and L. Kang, *J. Mater. Chem. A*, 2013, 1, 1380.
- 24 B. Senthilkumar, D. Meyrick, Y. S. Leec and R. K. Selvan, *RSC Adv.*, 2013, 3, 16542.
- 25 H. B. Gray, *Nat. Chem.*, 2009, 1, 7.
- 26 T. R. Cook, D. K. Dogutan, S. Y. Reece, Y. Surendranath, T. S. Teets and D. G. Nocera, *Chem. Rev.*, 2010, 110, 6474.
- 27 Y. Zhao, R. Nakamura, K. Kamiya, S. Nakanishi and K. Hashimoto, *Nat. Commun.*, 2013, 4, 2390.
- 28 F. Y. Cheng and J. Chen, *Chem. Society. Rev.*, 2012, 41, 2172.
- 29 J. Suntivich, K. J. May, H. A. Gasteiger, J. B. Goodenough and Y. S. Horn, *Science*, 2011, 334, 1383.
- 30 Y. Q. Guo, K. Xu, C. Z. Wu, J. Y. Zhao and Y. Xie, *Chem. Soc. Rev.*, 2015, 44, 637.
- 31 K. Xu, P. Z. Chen, X. L. Li, Y. Tong, H. Ding, X. J. Wu, W. S. Chu, Z. M. Peng, C. Z. Wu and Y. Xie, *J. Am. Chem. Soc.*, 2015, 137, 4119.
- 32 X. Y. Lu, W. L. Yim, B. H. R. Suryanto and C. Zhao, *J. Am. Chem. Soc.*, 2015, 137, 2901.
- 33 M. R. Gao, W. C. Sheng, Z. B. Zhuang, Q. R. Fang, S. Gu, J. Jiang and Y. S. Yan, *J. Am. Chem. Soc.*, 2014, 136, 7077.
- 34 W. Chen, H. T. Wang, Y. Z. Li, Y. Y. Liu, J. Sun, S. H. Lee, J. S. Lee and Y. Cui, *ACS Cent. Sci.*, 2015, 1, 244.
- 35 R. N. Singh, J. P. Singh and A. Singh, *Int. J. Hydrogen Energy*, 2008, 33, 4260.
- 36 R. N. Singh, Madhu, R. Awasthi and A. S. K. Sinha, *J. Solid State Electrochem.*, 2009, 13, 1613.
- 37 J. Zhao, Y. C. Zou, X. X. Zou, T. Y. Bai, Y. P. Liu, R. Q. Gao, D. J. Wang and G. D. Li, *Nanoscale*, 2014, 6, 7255.
- 38 Y. F. Zhao, S. Q. Chen, B. Sun, D. W. Su, X. D. Huang, H. Liu, Y. M. Yan, K. N. Sun and G. X. Wang, *Scientific reports*, 2015, 5, 7629.
- 39 H. Hu, B. Y. Guan, B. Y. Xia, and X. W. Lou, *J. Am. Chem. Soc.*, 2015, 137, 5590.
- 40 M. R. Gao, Y. F. Xu, J. Jiang, Y. R. Zheng and S. H. Yu, *J. Am. Chem.Soc.*, 2012, 134, 2930.
- 41 S. Chen and S. Z. Qiao, *Acs Nano*, 7, 10190.
- 42 H. Tüysüz, Y. J. Hwang, S. B. Khan, A. M. Asiri, and P. D. Yang, *Nano Res.*, 2013, 6, 47.
- 43 J. Wu, Yan Xue, X. Yan, W.S. Yan, Q. M. Cheng and Yi Xie, *Nano Res.*, 2012, 5, 521.
- 44 S. Q. Chen, Y. F. Zhao, B. Sun, Z. M. Ao, X.Q. Xie, Y. Y. Wei, and G. X. Wang, *ACS Appl. Mater. Int.*, 2015, 7, 3306.
- 45 S. Chen, J. J. Duan, M. Jaroniec and S. Z. Qiao, *Angew. Chem. Int. Ed.*, 2013, 52, 13567.
- 46 X. J. Liu, Z. Chang, L. Luo, T. H. Xu, X. D. Lei, J. F. Liu and X. M. Sun, *Chem. Mater.*, 2014, 26, 1889.
- 47 X. X. Zou, J. Su, R. Silva, A. Goswami, B. R. Satheab and T. Asefa, *Chem. commun.*, 2013, 49, 7522.
- 48 A. J. Esswein, M. J. McMurdo, P. N. Ross, A. T. Bell and T. D. Tilley, *J. Phys. Chem. C*, 2009, 113, 15068.
- 49 L. Fang, Y. Y. Shu, A. Wang and T. Zhang, *J. Phys. Chem. C*, 2007, 111, 2401.
- 50 Y. J. Chen, G. Xiao, T. S. Wang, F. Zhang, Y. Ma, P. Gao, C. L. Zhu, E. D. Zhang, Z. Xu and Q. H. Li, *Sens. Actuators, B*, 2011, 155, 270.
- 51 Q. S. Wang, Z. Y. Lei, Y. J. Chen, Q. Y. Ouyang, P. Gao, L. H. Qi, C. L. Zhu and J. Z. Zhang, *J. Mater. Chem. A*, 2013, 1, 11795.

Hierarchical nanosheet-based $\text{CoMoO}_4\text{-NiMoO}_4$ nanotubes exhibit superior electrochemical properties for applications in asymmetric supercapacitor and oxygen evolution reaction.

